Electromagnetic imaging through thick metallic enclosures

Brendan J. Darrer' , Joseph C. Watson, Paul A. Bartlett, and Ferruccio Renzoni

Citation: AIP Advances **5**, 087143 (2015); doi: 10.1063/1.4928864
View online: http://dx.doi.org/10.1063/1.4928864
View Table of Contents: http://aip.scitation.org/toc/adv/5/8
Published by the American Institute of Physics

AIP ADVANCES **5**, 087143 (2015)

Electromagnetic imaging through thick metallic enclosures

Brendan J. Darrer,[1,a] Joseph C. Watson,[2] Paul A. Bartlett,[1] and Ferruccio Renzoni[1]
[1]*Department of Physics & Astronomy, University College London, Gower Street, London, WC1E 6BT, United Kingdom*
[2]*Novel Detection Concepts, National Nuclear Security Programme, Atomic Weapons Establishment, Aldermaston, Reading, RG7 4PR, United Kingdom*

(Received 24 June 2015; accepted 5 August 2015; published online 14 August 2015)

The ability to image through metallic enclosures is an important goal of any scanning technology for security applications. Previous work demonstrated the penetrating power of electromagnetic imaging through thin metallic enclosures, thus validating the technique for security applications such as cargo screening. In this work we study the limits of electromagnetic imaging through metallic enclosures, considering the performance of the imaging for different thicknesses of the enclosure. Our results show, that our system can image a Copper disk, even when enclosed within a 20 mm thick Aluminum box. The potential for imaging through enclosures of other materials, such as Lead, Copper, and Iron, is discussed. © *2015 Author(s). All article content, except where otherwise noted, is licensed under a Creative Commons Attribution 3.0 Unported License.* [http://dx.doi.org/10.1063/1.4928864]

I. INTRODUCTION

Electromagnetic Induction Imaging (EII), closely related to the Eddy Current Array (ECA) technique[1,2] used in the nondestructive testing and Magnetic Induction Tomography (MIT),[4–11] is a non-contact imaging technique which relies on the establishment of eddy currents in a conductive sample via an applied alternating field, and the detection of the secondary magnetic field generated by these eddy currents. An important area of application of EII is in security. Previous work[3] demonstrated the penetrating power of EII through thin metallic enclosures, thus validating EII for security applications such as cargo screening. In this work we study the limits of EII through metallic enclosures, considering the performance of the imaging for different thicknesses of the enclosure. Our results show, that our EII system can detect a magnetic signature of a Copper disk, even when enclosed within a 20 mm thick Aluminum box.

This paper is organized as follows. First, the principles and technical details of our experimental system are described. Then, we report on an experiment to image through Aluminum enclosures of different thicknesses. The potential for imaging through four common metals is discussed. In the final section we summarize these results.

II. EXPERIMENTAL SET-UP

The set-up is the same as the one used in our previous work.[3,13]

The computer-automated set-up includes a Helmholtz-coil assembly (driver coils), with a planar array of 20×20 sensor coils placed on a platform between the two Helmholtz coils (Fig. 1). A near-to-uniform primary AC magnetic-field is established by a Helmholtz-coil assembly. The primary field, $\mathbf{B}$, excites eddy currents in the conductive sample-object, which generates its own opposing secondary-field, $\Delta\mathbf{B}$. The secondary field is detected by each sensor coil in the planar

[a]email: brendan.darrer.12@ucl.ac.uk

 ©Author(s) 2015

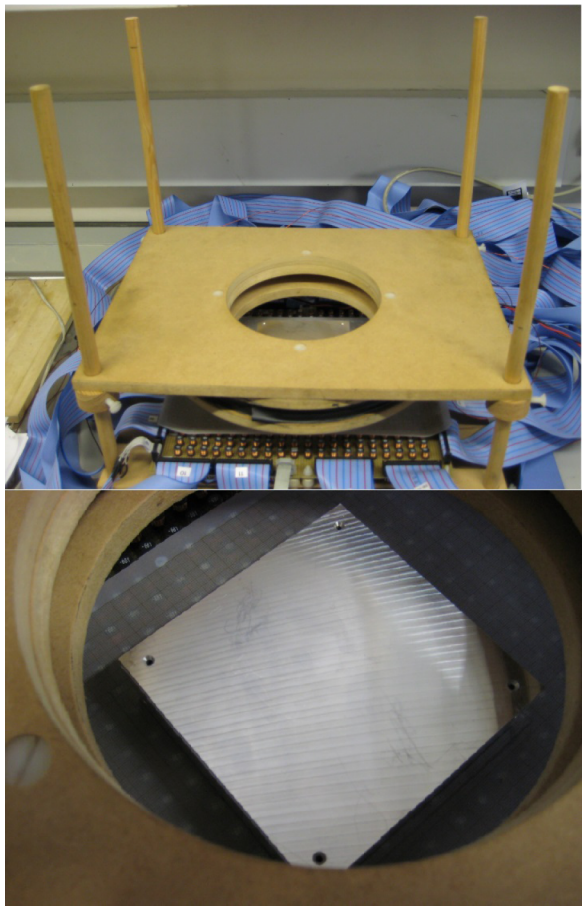

FIG. 1. Helmholtz-coil assembly and sensor-coil array (top). Aluminum box in position for imaging (bottom).

array. Imaging is achieved via phase-variation measurements between the signals of the driver and sensor coils, for each sensor-coil position. For the high conductivity and low permeability metallic-specimens examined here, the phase values are considered as related to the conductivity of the specimen only, i.e. conductivity-maps are generated.[4,12]

Table I shows the dimensions of these two types of coils, and Tables II and III give electromagnetic measurements of the coils at the frequencies used in the experiment.

The metallic specimen for imaging rests on top of the sensor array, separated by a sheet of graph paper, as shown in Fig. 1. A 150 W AC amplifier increases an oscillator signal to 27 V rms across the driver coils. This gives drive currents of 2.05 A rms, and a magnetic flux density at the level of the sensors as 2.9 mT rms at 10 Hz, with 21.4 mA and 0.03 mT rms at 2 kHz, as indicated in Table II. A Signal Recovery 7230 DSP dual-phase lock-in amplifier measures the voltage phase-difference between the driver and sensor coils. This is with the aid of an Agilent 34980A multiplexer, to automatically switch between 400 coils of the sensor-array, in 1 second intervals. The whole process is automated via LabVIEW, with the phase-difference data saved to an output file. The phase data matrix is concatenated with the positional data to generate an image of the metallic specimen. The resultant magnetic image is therefore a 2-dimensional surface plot of sensor-coil position in the x and y axes and voltage phase-difference on the z axis, as produced by performing a cubic piecewise-interpolation of the data.

III. IMAGING THROUGH ALUMINUM ENCLOSURES

In order to investigate the penetrating power of imaging through conductive enclosures, our experiment investigates imaging of a Copper disk through Aluminum enclosures of different thickness.

TABLE I. Dimensions of Helmholtz Coils and Sensor Coils.

Parameter	Measured Value
Helmholtz driver-coils	
External diameter	(28.7 ± 0.1) cm
Inner diameter	(25 ± 0.1) cm
Number of turns in each coil	300
Diameter of enameled Copper wire	(1.11 ± 0.02) mm
Perpendicular separation of the two coils from the vertical center of their windings	(13.5 ± 0.1) cm
Radius of each coil from horizontal center of their windings	(13.5 ± 0.1) cm
Vertical height of each coil	(1.85 ± 0.01) cm
Sensor coils	
External diameter	(6.90 ± 0.03) mm
Inner diameter	(3.6 ± 0.1) mm
Number of turns	146.5
Diameter of enameled Copper wire	(0.243 ± 0.001) mm
Vertical height of coil	(5.53 ± 0.05) mm
Spacing between center points of coils on array	(12.7 ± 0.5) mm
Size of sensor-coil array	(242 × 242) mm

TABLE II. Electrical And Magnetic Measurements Of Coils Between 10 Hz And 5 kHz.

Type of coil and frequency	Magnetic flux density at the level of the sensor coils (mT) rms	Current (mA)[a] rms	Potential difference (mV)[a] rms
Driver coils			
10 Hz	2.9 ± 0.6	2050 ± 80	(27 ± 1) V
40 Hz	1.8 ± 0.5	970 ± 40	“
200 Hz	0.4 ± 0.1	212 ± 8	“
1 kHz	0.07 ± 0.02	43 ± 2	“
2 kHz	0.03 ± 0.01	21.4 ± 0.8	“
5 kHz	[c]	8.4 ± 0.3	“
Sensor coil[b]			
10 Hz		(23.5 ± 0.5) μA	4.82 ± 0.09
40 Hz		(45 ± 1) μA	9.2 ± 0.2
200 Hz		(49 ± 1) μA	9.9 ± 0.2
1 k Hz		(48 ± 1) μA	9.8 ± 0.2
2 kHz		(48 ± 1) μA	9.8 ± 0.2
5 kHz		(48 ± 1) μA	9.8 ± 0.2

[a]Units of mV or mA unless otherwise stated.
[b]Average taken from 5 coils, includes 3 m of ribbon cable, and measurements were taken in the absence of any specimen.
[c]Measurement was too small to be read by the available gauss meter.

The choice of Copper is arbitrary. There is no reason at this stage to use different metal. However, an extended study could be undertaken to test different metallic specimens enclosed within the container.

We adopt the method of subtraction-of-phases of the full and empty enclosures.[13] The boxes are completely closed with sides, top and bottom of the same thickness, and a Copper disk concealed inside. All the boxes have a base of 10.5 cm by 10.5 cm and heights between 2.9 cm and 5 cm. Each was imaged at 6 different frequencies, 10 Hz to 5 kHz. The disk has 30 mm diameter and 2 mm thickness, in all the boxes except in the 20 mm box, where the disk is 40 mm diameter by 3 mm thickness, as the 30 mm disk could not be detected for this size of enclosure.

Representative images are reported in Fig. 2 and 3. Images that could not distinguish the disk were not included. This would be due to the box walls, being too deep in comparison to the skin

TABLE III. Resistance, Inductance And Impedance Of Coils Between 10 Hz And 5 kHz.

Type of coil and frequency	Resistance (Ω)	Inductance (mH)	Impedance (Ω)
Driver coil			
10 Hz	11.5 ± 0.1	101.1 ± 0.3[b]	13.14 ± 0.09
40 Hz	"	101.06 ± 0.09	27.90 ± 0.02
200 Hz	"	100.70 ± 0.03	127.10 ± 0.03
1 kHz	"	100.364 ± 0.004	630.76 ± 0.03
2 kHz	"	100.460 ± 0.002	1262.59 ± 0.02
5 kHz	"	101.921 ± 0.002	3202.37 ± 0.05
Sensor coil[a]			
10 Hz	205 ± 2	0.60 ± 0.04[b]	205 ± 2
40 Hz	"	0.62 ± 0.01	204.2 ± 0.9
200 Hz	"	0.615 ± 0.003	204.1 ± 0.9
1 k Hz	"	0.637 ± 0.002	204.1 ± 0.9
2 kHz	"	0.636 ± 0.002	204.3 ± 0.9
5 kHz	"	0.635 ± 0.002	205.3 ± 0.9

[a]Average taken from 5 coils, includes 3 m of ribbon cable.
[b]20 Hz inductance value.

depth, at the applied frequency. These results demonstrate that an image of the concealed disk could be extracted, from five Aluminum box-enclosures of 2 mm to 20 mm wall thickness. This was achieved at frequencies 10 Hz to 5 kHz, for the 2 mm and 3 mm thick boxes (Fig. 2(ai) to 3(aii) and 2(bi) to 3(biii)); at 10 Hz to 2 kHz for the 5 mm box (Fig. 2(ci) to 3(cii)); and 10 to 200 Hz for the 10 to 20 mm thick boxes (Fig. 2(di) to 2(eiii)).

Clearer disk-images were obtained at the mid-range frequencies, 40 Hz to 1 kHz, for box thicknesses that were not too large, i.e. 2 mm to 5 mm.

At lower frequency, and specifically 10 Hz, penetration of the driving field was sufficient to image the concealed disk, for all thicknesses of the box-enclosures, however the image was unstable and fluctuated. We attribute this, as due to smaller eddy currents induced in the specimen, giving a weaker potential-difference across the sensors (see Table II). It was also noticed that at 10 Hz, the primary field is at its largest value of 2.9 mT (rms) (Table II) due to the low impedance of the Helmholtz coils (Table III). A background image with no specimen present also shows instability at this frequency. At 10 Hz the strength of the source magnetic field is significantly reduced, and therefore at such a frequency there is not enough power in the field to excite enough eddy currents in the sample object, to generate a stabilized phase image.

The skin depth[14] of the Aluminum enclosure and the enclosed Copper disk, determines our ability to image through the enclosure. This is demonstrated by the images of Fig. 2 to 3. The disk-images change shape slightly for the different thickness of the enclosure, but the overall shape remains consistent for different frequencies of the applied signals; except for the 10 and 20 mm thick boxes, which gave varying shapes within the same overall location of the actual disk. The edges of the disk-image can be observed in some of the images between 10 to 200 Hz, notably Fig. 2(aii), 2(aiii), 2(cii) and 2(ciii). The image peaks at these frequencies in the disk-center and drops in phase below the background at the edges, due to the electrical field being concentrated there.[15] For frequencies of 1 kHz to 5 kHz, the phase values gave the opposite effect, dipping to lower values for the disk-center and rising above the background at the edges as shown in Fig. 3(ai), 3(ci) and 3(cii). The absence of edge effects in some of the mages could have been caused when removing the lid to place the disk inside, so that the full and empty enclosures were not identically-repositioned. An additional cause may be the instability of the image. The 5 kHz image of the 3 mm Aluminum box gave a peaked image as opposed to a dipped image. It was noted that the two 5 kHz images shown, exhibited instability. This could be due to the very small magnetic field from the driver coils at this frequency, because the high impedance produces a much smaller current in the driver coils (Table II & III). Additionally, there is the factor due to the small skin depth at this frequency. The 5 kHz image for the 2 mm thick box shows strong image-artifacts,

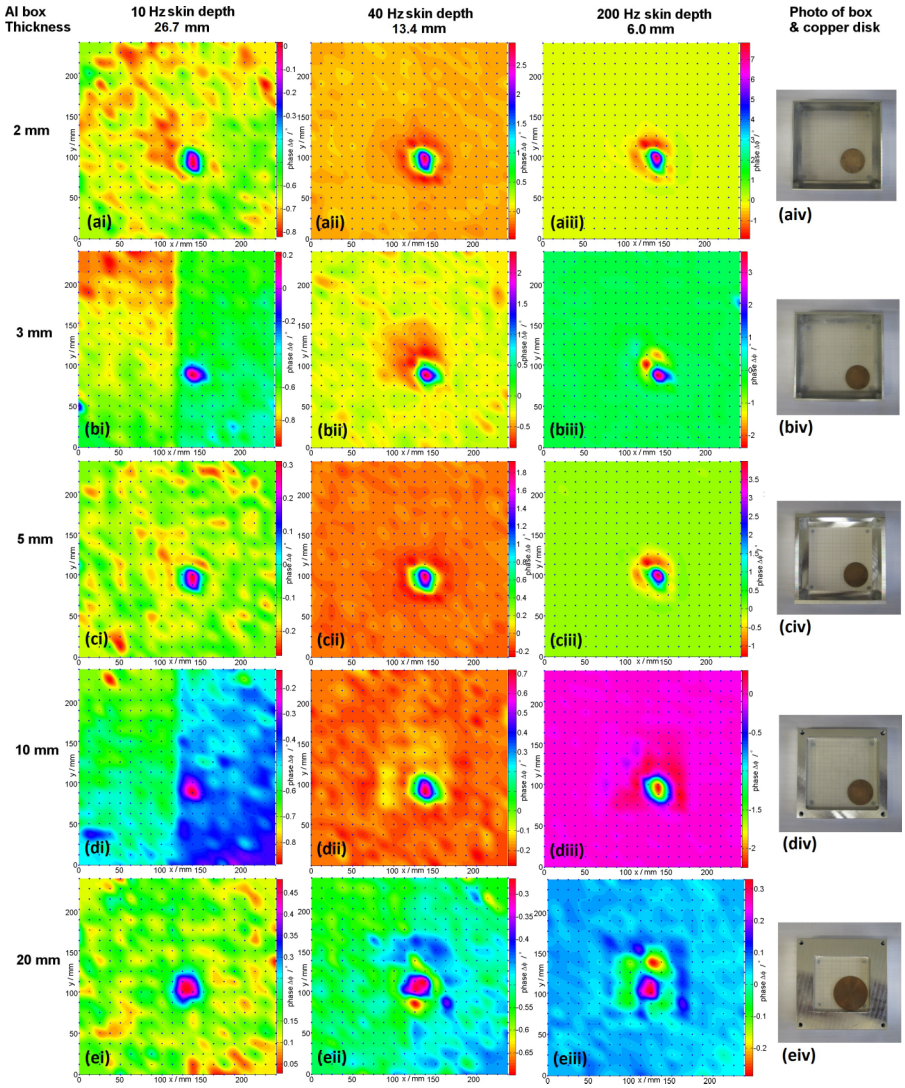

FIG. 2. Magnetic image capture of a Copper disk concealed inside five separate Aluminum (Al) box-enclosures of thicknesses, 2 mm to 20 mm. Images were captured at frequencies of 10 to 200 Hz, with x and y axes showing 2D position in mm, and the z axis representing the phase values in degrees. Images are displayed as a table, showing box thickness with respect to frequency and skin depth, in (ai to eiii), and aerial photograph of the boxes with concealed disk, in (aiv to eiv). Photographs show Aluminum boxes with the lid off, but images were taken with the lid on.

revealing the edge of the box, higher up in the image. The 2 mm box image was captured many times at 5 kHz, but due to its light weight, it was vulnerable to being disturbed when removing and replacing back its lid. The images through 10 to 20 mm thick boxes, at frequency $\geq$ 1 kHz, were too fragmented and did not register the presence of the disk, as the skin depth, δ, varied between 2.69 to 1.2 mm, in the considered range of frequencies. The skin depth was therefore too small compared with the box thickness, thus denying penetration of the primary field.

The significant result presented in this work is that our EII system has been able to penetrate an Aluminum enclosure of 20 mm wall thickness, and that a magnetic signature of the disk can still be detected, even when the primary field has passed through 40 mm of Aluminum and a Copper disk of 40 mm diameter by 3 mm thickness. This was achieved at 10 to 200 Hz driving fields.

To quantify the penetrating power of our imaging system, we refer to the number of skin depths we can penetrate at a given frequency, to capture an image of the object inside the enclosure. Tables IV and V summarize our results for the depth of penetration at the different frequencies,

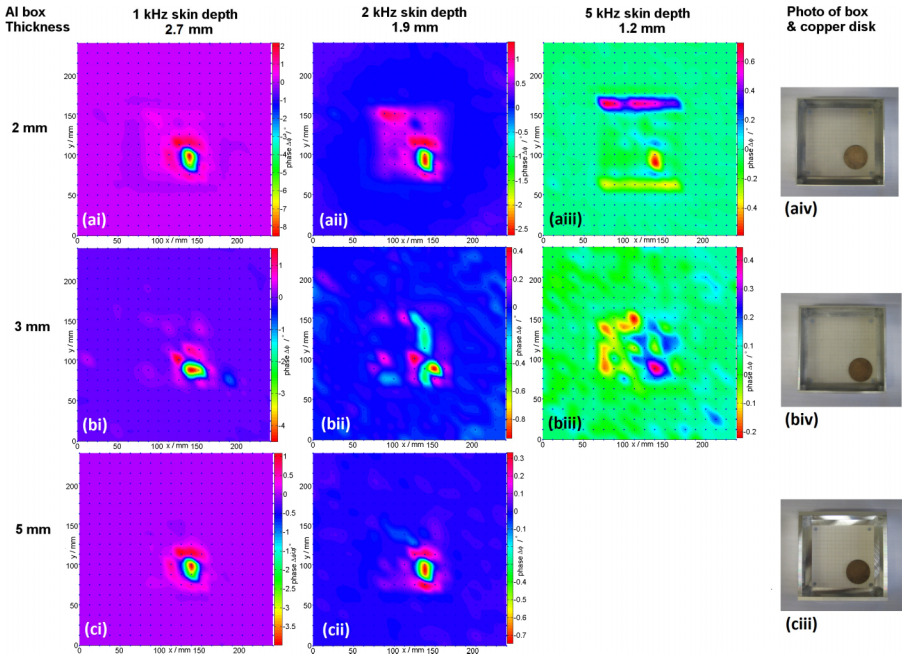

FIG. 3. Magnetic image capture of a Copper disk concealed inside three separate Aluminum (Al) box-enclosures of thicknesses, 2 mm to 5 mm. Images were captured at frequencies of 1 to 5 kHz, with x and y axes showing 2D position in mm, and the z axis representing the phase values in degrees. Images are displayed as a table, showing box thickness with respect to frequency and skin depth, in (ai to cii) and aerial photograph of the boxes with concealed disk, in (aiv to ciii). Photographs show Aluminum boxes with the lid off, but images were taken with the lid on.

TABLE IV. Number of Skin Depths Penetrated at Frequency 10 To 200 Hz.

Al box thickness	10 Hz n	40 Hz n	200 Hz n
2 mm	0.245	0.491	1.10
3 mm	0.320	0.640	1.43
5 mm	0.470	0.939	2.10
10 mm	0.844	1.69	3.77
20 mm	1.64	3.28	7.33

TABLE V. Number of Skin Depths Penetrated at Frequency 1 To 5 kHz.

Al box thickness	1 kHz n	2 kHz n	5 kHz n
2 mm	2.45	3.47	5.48
3 mm	3.20	4.53	7.16
5 mm	4.70	6.64	

as corresponding to the successful capture of an image. The penetration depth is given in terms of number n of skin depths, reported in units of the Al skin depth δ[14] for each frequency. The penetration depth includes the contributions from the top and bottom sides of the Aluminum box, each of thickness x_2, as well as from the Copper (Cu) disk enclosed, of thickness x_1. The number of skin depths n penetrated at a given frequency is given by $n = 2x_2/\delta + x_1/\delta_{Cu}$, where δ_{Cu} is the skin depth of Copper at the frequency of interest.

A more practical technique, that does not require opening the enclosure and removing its contents, is the dual-frequency method, described in Ref. 3. This method relies on a low frequency

image to penetrate the enclosure and a high frequency image to approximate the empty enclosure. While this technique works for conductive enclosures of 0.24 mm and 0.33 mm thickness, it does not appear to work for Aluminum boxes of ≥ 2mm thickness. This is because the high frequency image generates peaks of phase, that are not consistent with the low frequency image, and therefore the extraction of the concealed disk is rendered invalid. The identification of the exact mechanisms behind such a behavior will constitute the object of a separate investigation.

IV. POTENTIAL FOR IMAGING THROUGH OTHER MATERIALS

Our work dealt specifically with Aluminum enclosures and Copper disks. However from our results we can tentatively extrapolate the potential for imaging through metal shields of different materials.

Fig. 4 displays a log-log plot of skin depth versus frequency for 4 common metals, Aluminum, Copper, Iron (99.95% pure in 2 mT field) and Lead.[16] Indicated in the plot, in blue, is the range of frequencies used in the present experiment, 10 Hz to 5 kHz. As from the plot, Copper is less penetrable than Aluminum, whereas greater penetrability is associated with Lead. Iron (99.95%) shows a much poorer penetration due to its larger relative permeability of $\mu_r \sim 5 \times 10^3$. A slightly less pure Iron (99.91% pure in 2 mT field) has μ_r equal to 200, and is therefore more penetrable.

We recall that the results presented in this paper have shown 7.33 skin depths were penetrated for imaging through the 20 mm Al box at 200 Hz. Beyond this value there is no visible detection of the Copper disk. This result for the penetration depth of imaging, and relative optimum frequency, will be used to discuss the potential for imaging through other materials.

Using Fig. 4 it is possible to extrapolate the thickness of Fe, Cu and Pb enclosures through which imaging should be possible with our current set-up. For a given material M of skin depth δ_M at the imaging frequency, seven skin depths ($n = 7$) correspond to a thickness of the enclosure equal to x_2 in (1),

$$x_2 = \left(n - \frac{x_1}{\delta_{Cu}}\right)\frac{\delta_M}{2} = \left(7 - \frac{x_1}{\delta_{Cu}}\right)\frac{\delta_M}{2} \tag{1}$$

where x_1 is the thickness of the Copper disk and δ_{Cu} the skin depth of Copper at the imaging frequency. As discussed above, we adopt 200 Hz as the reference frequency to determine the

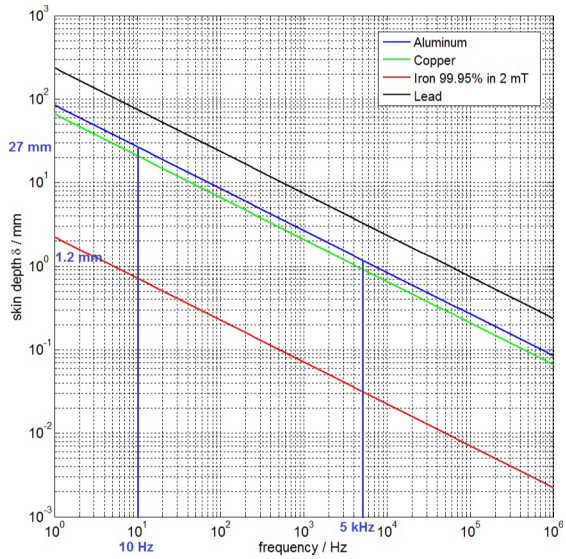

FIG. 4. Log-log plot of skin depth versus frequency for 4 common metals, Aluminum, Copper, Iron (99.95% purity in 2 mT field) and Lead. The frequency range of the experiment is indicated in blue on the x axis, along with the corresponding skin depth (δ) values, in blue, on the y axis.

maximum thickness of the different materials through which the set-up should be able to image. Proceeding as detailed above, we identify the potential for imaging through enclosure of thickness 54.8 mm for Pb, 0.52 mm for Fe (99.95% pure in 2 mT field) and 15.4 mm for Cu.

V. CONCLUSION

We have investigated the limits of magnetic imaging through metallic enclosures, analyzing the performance of imaging for different thickness of the enclosure. Our results show, that our system can image a Copper disk, even when enclosed within a 20 mm thick Aluminum box. On the basis of the reported results, we discussed the potential for imaging through different conductive materials.

The results presented here demonstrate the penetrating power of our system, and are of relevance to security applications such as cargo screening.

ACKNOWLEDGMENT

This work was jointly funded by AWE and UCL via the PhD studentship Impact scheme.
© British Crown Copyright AWE/2015.

[1] E. Pelletier, M. Grenier, A. Chahbaz, and T. Bourgelas, "Array Eddy Current for Fatigue Crack Detection of Aircraft Skin Structures," in Proc. Vth International Workshop, Advances in Signal Processing for Non Destructive Evaluation of Materials, Québec City, 2-4 Aug. 2005.
[2] L. Bo, L. Feilu, J. Zhongqing, and L. Jiali, "Eddy Current Array Instrument and Probe for Crack Detection of Aircraft Tubes," in *IEEE International Conference on Intelligent Computation Technology and Automation* (2010).
[3] B. J. Darrer, J. C. Watson, P. A. Bartlett, and F. Renzoni, "Magnetic imaging: a new tool for UK national nuclear security," Sci. Rep. **5**, 7944 (2015) [Online]. Available: http://www.nature.com/srep/2015/150122/srep07944/full/srep07944.html.
[4] H. Griffiths, "Magnetic induction tomography," Meas. Sci. Technol **12**(8), 1126–1131 (2001).
[5] A.V. Korjenevsky, V.A. Cherepenin, and S. Sapetsky, "Magnetic induction tomography: experimental realization," Physiol. Meas. **21**(1), 89–91 (2000).
[6] A.V. Korjenevsky and V.A. Cherepenin, "Magnetic induction tomography," J. Commun. Technol. Electron. **42**(4), 469–474 (1997).
[7] L. Ma, H-Y. Wei, and M. Soleimani, "Planar magnetic induction tomography for 3D near subsurface imaging," Prog. Electromagn. Res. **138**, 65–82 (2013).
[8] X. Ma, A. J. Peyton, M. Soleimani, and W. R. B. Lionheart, "Imaging internal structure with electromagnetic induction tomography. Presented at Instrumentation and Measurement Technology Conference" (2006, April) [Online]. Available: http://ieeexplore.ieee.org/xpl/articleDetails.jsp?arnumber=4124330&tag=1.
[9] A. J. Peyton, M. S. Beck, A. R. Borges, J. E. de Oliveira, G. M. Lyon, Z. Z. Yu, M. W. Brown, and J. Ferrerra, "Development of electromagnetic tomography (EMT) for industrial applications. Part 1: sensor design and instrumentation," in *WCIPT1*, *Greater Manchester*, *1999*. p. 306.
[10] M. Soleimani, "Simultaneous reconstruction of permeability and conductivity in magnetic induction tomography," J. of Electromagn. Waves and Appl **23**(5/6), 785 (2009).
[11] H-Y. Wei and M. Soleimani, "A magnetic induction tomography system for prospective industrial processing applications," Chin. J. Chem. Eng. **20**(2), 406 (2012).
[12] H. Griffiths, W. Gough, S. Watson, and R. J. Williams, "Residual capacitive coupling and the measurement of permittivity in magnetic induction tomography," Physiol. Meas. **28**(7), S301–S311 (2007).
[13] B. J. Darrer, J. C. Watson, P. A. Bartlett, and F. Renzoni, "Toward an automated setup for magnetic induction tomography," IEEE Trans. Magn. **51**(1), (2015).
[14] H. A. Wheeler, "Formulas for the skin effect," Proc. IRE **30**(9), 415 (1942).
[15] G. R. Quinn, "Eddy current testing," in *Handbook of Nondestructive Evaluation*, edited by C. J. Hellier (McGraw-Hill, New York, 2003), p. 8.19 Chap. 8, sec. 4.1.
[16] *CRC handbook of chemistry and physics: A ready-reference book of chemical and physical data*, 60th ed., (CRC, Boca Raton, Florida, 1981), pp. E-85 - E-125.